Int J Fract (2018) 213:1–16
https://doi.org/10.1007/s10704-018-0302-y

ORIGINAL PAPER

The configurational-forces view of the nucleation and propagation of fracture and healing in elastomers as a phase transition

Aditya Kumar · K. Ravi-Chandar · Oscar Lopez-Pamies

Received: 2 March 2018 / Accepted: 17 July 2018 / Published online: 31 July 2018

Abstract In a recent contribution, Kumar et al. (J Mech Phys Solids 112:523–551, 2018) have introduced a macroscopic theory aimed at describing, explaining, and predicting the nucleation and propagation of fracture and healing in elastomers undergoing arbitrarily large quasistatic deformations. The purpose of this paper is to present an alternative derivation of this theory—originally constructed as a generalization of the variational theory of brittle fracture of Francfort and Marigo (J Mech Phys Solids 46:1319–1342, 1998) to account for physical attributes innate to elastomers that have been recently unveiled by experiments at high spatio-temporal resolution—cast as a phase transition within the framework of configurational forces. A second objective of this paper is to deploy the theory to probe new experimental results on healing in silicone elastomers.

Keywords Cavitation · Self-healing polymers · Finite deformations

Electronic supplementary material The online version of this article (https://doi.org/10.1007/s10704-018-0302-y) contains supplementary material, which is available to authorized users.

A. Kumar · O. Lopez-Pamies (✉)
Department of Civil and Environmental Engineering, University of Illinois, Urbana–Champaign, Urbana, IL 61801-2352, USA
e-mail: pamies@illinois.edu

A. Kumar
e-mail: akumar51@illinois.edu

K. Ravi-Chandar
Department of Aerospace and Engineering Mechanics, The University of Texas at Austin, Austin, TX 78712–1221, USA
e-mail: ravi@utexas.edu

1 Introduction

The recent analysis by Lefèvre et al. (2015) of the classical experiments of Gent and Lindley (1959) and Gent and Park (1984), and the companion analyses by Poulain et al. (2017, 2018) of analogous new experiments at higher spatio-temporal resolution have unveiled a complete qualitative picture of the processes of nucleation and propagation of internal fracture and healing in elastomers subjected to externally applied quasistatic mechanical loads. In an attempt to gain precise quantitative insight into these fundamental phenomena, Kumar et al. (2018) have put forth a macroscopic theory that addresses the nucleation and propagation of fracture and healing in elastomers on an equal footing as a phase transition. Specifically, this theory is based on two core ideas. The first one is to view elastomers as solids capable to undergo finite elastic deformations and capable also to phase transition to another solid of vanishingly small stiffness—whereas the forward phase transition serves to characterize the nucleation and propagation of fracture, the reverse phase transition characterizes the possible healing. The second core idea is to take the phase transi-

tion to be driven by the competition between a combination of strain energy and hydrostatic stress concentration in the *bulk* and surface energy on the created/healed new *surfaces* in the elastomer. By construction, the theory introduced in Kumar et al. (2018) can be thought of as a generalization of the celebrated variational theory of brittle fracture of Francfort and Marigo (1998), or, more precisely, a generalization of its regularized version—where cracks are not sharp, but rather, diffuse interfaces—put forth in Bourdin et al. (2000, 2008).

The purpose of this paper is to present an alternative derivation of the theory of Kumar et al. (2018) as a theory of phase transition cast within the framework of configurational forces. In addition to furnishing a different and physically enriching perspective, this alternative derivation provides a framework that makes it plain how to generalize systematically the theory to account for dissipative phenomena that go beyond those associated with the fracturing and the healing, e.g., viscous dissipation[1]. A second objective of this paper is to deploy the theory to examine the new experimental results on the healing of silicone elastomers reported in Poulain et al. (2018).

To bring clarity to the various physical mechanisms summoned in the proposed alternative derivation, we begin in Sect. 2 by presenting a fairly general constitutive framework for finitely deformable solids that are capable of solid-to-solid phase transition. The framework follows the approach of configurational forces wherein an order parameter or configurational scalar field is utilized to identify the various phases of the solid and a balance of configurational forces is used to describe the evolution of such an order parameter (Fried and Gurtin 1994; Gurtin 1996). Additionally, the framework features internal variables that serve to describe dissipative phenomena other than those associated with phase transition. A defining ingredient of the proposed formulation is that the constitutive response of the solid is expediently described by two thermodynamic potentials: a free-energy function and a dissipation potential. While the latter characterizes how the solid dissipates energy through mechanical deformation, phase transition, and possibly other mechanisms, the former characterizes how it stores energy (see, e.g., Ziegler and Wehrli 1987; Nguyen and Andrieux 2005; Kumar and Lopez-Pamies 2016). In Sect. 3, we re-derive the theory of Kumar et al. (2018) in the general context of N space dimensions as a special case of the constitutive framework put forth in Sect. 2. Finally, we devote Sect. 4 to confront the theory with the experiments on healing.

2 A constitutive framework for deformable solids capable of solid-to-solid phase transition

2.1 Kinematics

Consider a solid that occupies in its initial configuration (at time $t = 0$) a bounded domain $\Omega_0 \subset \mathbb{R}^N$, with boundary $\partial\Omega_0$ and unit outward normal $\mathbf{N}$. We identify material points by their initial position vector $\mathbf{X} \in \Omega_0$. At a later time $t \in (0, T]$, due to externally applied stimuli to be described below, the position vector $\mathbf{X}$ of a material point moves to a new position specified by

$$\mathbf{x} = \mathbf{y}(\mathbf{X}, t),$$

where $\mathbf{y}$ is a mapping from Ω_0 to the current configuration $\Omega(t)$, also contained in $\mathbb{R}^N$. We consider only invertible deformations, and write the deformation gradient and particle velocity fields at $\mathbf{X}$ and t as

$$\mathbf{F}(\mathbf{X}, t) = \text{Grad}\, \mathbf{y}(\mathbf{X}, t) \qquad \text{and} \qquad \dot{\mathbf{y}}(\mathbf{X}, t) = \frac{\partial \mathbf{y}}{\partial t}(\mathbf{X}, t). \tag{1}$$

The solid comprises two[2] different solid phases which may phase transition from one to the other in response to the external stimuli. We make use of an order parameter or configurational scalar field

$$z(\mathbf{X}, t)$$

to identify the two phases and, akin to (1), write the gradient and the rate of change of z at $\mathbf{X}$ and t as

$$\mathbf{Z}(\mathbf{X}, t) = \text{Grad}\, z(\mathbf{X}, t) \text{ and } \dot{z}(\mathbf{X}, t) = \frac{\partial z}{\partial t}(\mathbf{X}, t).$$

[1] In addition to elastic deformations, viscous deformations are likely to play a role in the nucleation and propagation of fracture and healing in elastomers; see, e.g., Mullins (1959) and Kumar et al. (2017).

[2] The extension of the present formulation to the case of any number of phases is straightforward.

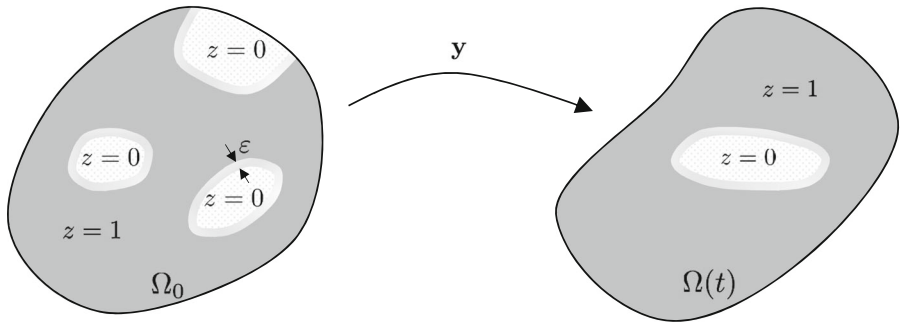

Fig. 1 Schematics of the solid in its initial configuration at time $t = 0$ and in a deformed configuration, described by the mapping $\mathbf{y}(\mathbf{X}, t)$, at a later time $t > 0$. The schematics also show the coexistence and evolution of the two phases, identified by the values 1 and 0 of the configurational variable $z(\mathbf{X}, t)$, making up the solid, as well as the thin inter-phase regions of length scale ε separating them, wherein $0 < z < 1$

We choose to set $z = 1$ in regions occupied by one phase, and $z = 0$ in regions occupied by the other. In a sharp interface formulation, the field z would only take the value of 1 or 0 at any given material point and hence would be discontinuous at interfaces separating the regions occupied by the two different phases. In this work, we adopt a regularized formulation featuring diffuse interfaces in which the configurational variable z is allowed to vary smoothly from 1 to 0 over thin inter-phase regions of length scale ε. Figure 1 shows schematics of the solid in its initial configuration and at a later time, illustrating the coexistence and evolution of the two solid phases and the thin inter-phase regions separating them.

2.2 Constitutive behavior

The constitutive behavior of the solid is taken to be characterized by two thermodynamic potentials that describe how the solid stores and dissipates energy through deformation, phase transition, and possibly other mechanisms[3]: (*i*) a free-energy function ψ and (*ii*) a dissipation potential ϕ. While more general dependencies and functional forms are possible, we take here

$$\psi = \psi(\mathbf{F}, z, \mathbf{Z}, \boldsymbol{\alpha}) \quad \text{and} \quad \phi = \phi(\mathbf{F}, z, \mathbf{Z}, \boldsymbol{\alpha}, \dot{z}, \dot{\mathbf{Z}}, \dot{\boldsymbol{\alpha}}), \tag{2}$$

where $\boldsymbol{\alpha} = \boldsymbol{\alpha}(\mathbf{X}, t)$ stands for a finite number of internal variables that serve to account for dissipative mechanisms other than those associated with the transition between phases (e.g., viscous dissipation), and where $\dot{\mathbf{Z}}(\mathbf{X}, t) = \partial \mathbf{Z}(\mathbf{X}, t)/\partial t$ and $\dot{\boldsymbol{\alpha}}(\mathbf{X}, t) = \partial \boldsymbol{\alpha}(\mathbf{X}, t)/\partial t$. We emphasize that the inclusion of $\mathbf{Z}$ as argument in the above thermodynamic potentials is the simplest constitutive choice to account for the regularization of the configurational variable z (e.g., higher-order gradients of z could also be included as arguments), but one that is sufficiently general to describe a wide range of phenomena, including the fracture and healing phenomena in elastomers of interest in this work. Material frame indifference requires that $\psi(\mathbf{QF}, z, \mathbf{Z}, \boldsymbol{\alpha}) = \psi(\mathbf{F}, z, \mathbf{Z}, \boldsymbol{\alpha})$ and $\phi(\mathbf{QF}, z, \mathbf{Z}, \boldsymbol{\alpha}, \dot{z}, \dot{\mathbf{Z}}, \dot{\boldsymbol{\alpha}}) = \phi(\mathbf{F}, z, \mathbf{Z}, \boldsymbol{\alpha}, \dot{z}, \dot{\mathbf{Z}}, \dot{\boldsymbol{\alpha}})$ for all $\mathbf{Q} \in Orth^+$ and arbitrary $\mathbf{F}$, z, $\mathbf{Z}$, $\boldsymbol{\alpha}$. The second law of thermodynamics requires further that the free-energy function and dissipation potential satisfy the constraint

$$\dot{z}\,\frac{\partial \phi}{\partial \dot{z}}(\mathbf{F}, z, \mathbf{Z}, \boldsymbol{\alpha}, \dot{z}, \dot{\mathbf{Z}}, \dot{\boldsymbol{\alpha}}) + \dot{\mathbf{Z}} \cdot \frac{\partial \phi}{\partial \dot{\mathbf{Z}}}(\mathbf{F}, z, \mathbf{Z}, \boldsymbol{\alpha}, \dot{z}, \dot{\mathbf{Z}}, \dot{\boldsymbol{\alpha}}) - \dot{\boldsymbol{\alpha}} \cdot \frac{\partial \psi}{\partial \boldsymbol{\alpha}}(\mathbf{F}, z, \mathbf{Z}, \boldsymbol{\alpha}) \geq 0$$

for arbitrary $\mathbf{F}$, z, $\mathbf{Z}$, $\boldsymbol{\alpha}$.

Given the thermodynamic potentials (2), and the constraints above, it follows from standard arguments that the first Piola-Kirchhoff stress tensor $\mathbf{S}$ at any material point $\mathbf{X} \in \Omega_0$ and time $t \in [0, T]$ is conveniently given in terms of the deformation gradient tensor $\mathbf{F}$, configurational variables z and $\mathbf{Z}$, and internal variables $\boldsymbol{\alpha}$ by the relation

$$\mathbf{S}(\mathbf{X}, t) = \frac{\partial \psi}{\partial \mathbf{F}}(\mathbf{F}, z, \mathbf{Z}, \boldsymbol{\alpha}). \tag{3}$$

[3] Throughout this work, we focus on isothermal processes.

In turn, the combination of partial derivatives[4]

$$c_{\mathtt{i}}(\mathbf{X},t) = -\frac{\partial \psi}{\partial z}(\mathbf{F},z,\mathbf{Z},\boldsymbol{\alpha}) - \frac{\partial \phi}{\partial \dot{z}}(\mathbf{F},z,\mathbf{Z},\boldsymbol{\alpha},\dot{z},\dot{\mathbf{Z}},\dot{\boldsymbol{\alpha}})$$

and

$$\mathbf{C}(\mathbf{X},t) = \frac{\partial \psi}{\partial \mathbf{Z}}(\mathbf{F},z,\mathbf{Z},\boldsymbol{\alpha}) + \frac{\partial \phi}{\partial \dot{\mathbf{Z}}}(\mathbf{F},z,\mathbf{Z},\boldsymbol{\alpha},\dot{z},\dot{\mathbf{Z}},\dot{\boldsymbol{\alpha}}) \tag{4}$$

provide the constitutive relations at any material point $\mathbf{X} \in \Omega_0$ and time $t \in [0,T]$ between $\mathbf{F}$, z, $\mathbf{Z}$, $\boldsymbol{\alpha}$ and the configurational *internal* force $c_{\mathtt{i}}$ and the configurational stress $\mathbf{C}$, conjugate to the configurational variables z and $\mathbf{Z}$. In the constitutive relations (3) and (4), for definiteness, we take the internal variables $\boldsymbol{\alpha}$ to be implicitly defined by an evolution equation in the form of a system of first-order nonlinear ordinary differential equations. Formally, we write

$$\mathcal{A}\{\dot{\boldsymbol{\alpha}},\boldsymbol{\alpha};\mathbf{F},z,\mathbf{Z}\} = \mathbf{0} \tag{5}$$

with initial condition $\boldsymbol{\alpha}(\mathbf{X},0) = \boldsymbol{\alpha}_0(\mathbf{X})$.

2.3 Boundary conditions and source terms

We now specify the external stimuli applied to the solid, which comprise both prescribed boundary data and source terms in the bulk.

Thus, on a portion $\partial\Omega_0^{\mathbf{y}}$ of the boundary $\partial\Omega_0$, the deformation field $\mathbf{y}$ is taken to be given by a known function $\boldsymbol{\xi}$, while the complementary part of the boundary $\partial\Omega_0^{\mathbf{S}} = \partial\Omega_0 \backslash \partial\Omega_0^{\mathbf{y}}$ is subjected to a prescribed nominal traction $\mathbf{SN} = \boldsymbol{\sigma}$. Moreover, the value of the configurational variable z is taken to be given by a known function ω on a portion $\partial\Omega_0^z$ (possibly different from $\partial\Omega_0^{\mathbf{y}}$ and $\partial\Omega_0^{\mathbf{S}}$) of the boundary $\partial\Omega_0$, while the complementary portion $\partial\Omega_0^{\mathbf{C}} = \partial\Omega_0 \backslash \partial\Omega_0^z$ is subjected to a prescribed flux $\mathbf{C}\cdot\mathbf{N} = \tau$. More specifically, we consider the boundary conditions

$$\begin{aligned} &\mathbf{y} = \boldsymbol{\xi}(\mathbf{X},t), \quad (\mathbf{X},t) \in \partial\Omega_0^{\mathbf{y}} \times [0,T], \\ &\mathbf{SN} = \boldsymbol{\sigma}(\mathbf{X},t), \quad (\mathbf{X},t) \in \partial\Omega_0^{\mathbf{S}} \times [0,T], \end{aligned} \tag{6}$$

and

$$\begin{aligned} &z = \omega(\mathbf{X},t), \quad (\mathbf{X},t) \in \partial\Omega_0^{z} \times [0,T], \\ &\mathbf{C}\cdot\mathbf{N} = \tau(\mathbf{X},t), \quad (\mathbf{X},t) \in \partial\Omega_0^{\mathbf{C}} \times [0,T]. \end{aligned} \tag{7}$$

Throughout Ω_0, we also consider that the solid is subjected to a body force and a configurational *external* force

$$\mathbf{b}(\mathbf{X},t) \text{ and } c_{\mathtt{e}}(\mathbf{X},t), \quad (\mathbf{X},t) \in \Omega_0 \times [0,T]. \tag{8}$$

2.4 Governing equations

At this stage, we are in a position to spell out the equations that govern the mechanical response and phase transition of the above-described solid when subjected to the time-dependent boundary data (6)–(7) and source terms (8). Indeed, in the absence of inertial effects and upon substitution of the constitutive relations (3)–(5) in the equations of balance of linear momentum and balance of configurational forces (see, e.g., Fried and Gurtin 1994; Gurtin 1996),

$$\operatorname{Div}\mathbf{S} + \mathbf{b} = \mathbf{0}$$

and

$$\operatorname{Div}\mathbf{C} + c_{\mathtt{i}} + c_{\mathtt{e}} = 0,$$

and in the boundary conditions (6)–(7), the governing equations for the solid reduce to the following coupled system of boundary-value problems

$$\begin{cases} \operatorname{Div}\left[\dfrac{\partial \psi}{\partial \mathbf{F}}(\mathbf{F},z,\mathbf{Z},\boldsymbol{\alpha})\right] + \mathbf{b}(\mathbf{X},t) = \mathbf{0}, & (\mathbf{X},t) \in \Omega_0 \times [0,T] \\ \mathbf{y}(\mathbf{X},t) = \boldsymbol{\xi}(\mathbf{X},t), & (\mathbf{X},t) \in \partial\Omega_0^{\mathbf{y}} \times [0,T] \\ \left[\dfrac{\partial \psi}{\partial \mathbf{F}}(\mathbf{F},z,\mathbf{Z},\boldsymbol{\alpha})\right]\mathbf{N} = \boldsymbol{\sigma}(\mathbf{X},t), & (\mathbf{X},t) \in \partial\Omega_0^{\mathbf{S}} \times [0,T] \end{cases} \tag{9}$$

[4] The partial derivative with respect to the configurational variable z should be interpreted as a constrained derivative since $0 \le z \le 1$.

and

$$\begin{cases} \mathrm{Div}\left[\dfrac{\partial \psi}{\partial \mathbf{Z}}(\mathbf{F}, z, \mathbf{Z}, \boldsymbol{\alpha}) + \dfrac{\partial \phi}{\partial \dot{\mathbf{Z}}}(\mathbf{F}, z, \mathbf{Z}, \boldsymbol{\alpha}, \dot{z}, \dot{\mathbf{Z}}, \dot{\boldsymbol{\alpha}})\right] + c_{\mathrm{e}}(\mathbf{X}, t) \\ = \dfrac{\partial \psi}{\partial z}(\mathbf{F}, z, \mathbf{Z}, \boldsymbol{\alpha}) + \dfrac{\partial \phi}{\partial \dot{z}}(\mathbf{F}, z, \mathbf{Z}, \boldsymbol{\alpha}, \dot{z}, \dot{\mathbf{Z}}, \dot{\boldsymbol{\alpha}}), & (\mathbf{X}, t) \in \Omega_0 \times [0, T] \\ z(\mathbf{X}, t) = \omega(\mathbf{X}, t), & (\mathbf{X}, t) \in \partial\Omega_0^z \times [0, T] \\ \left[\dfrac{\partial \psi}{\partial \mathbf{Z}}(\mathbf{F}, z, \mathbf{Z}, \boldsymbol{\alpha}) + \dfrac{\partial \phi}{\partial \dot{\mathbf{Z}}}(\mathbf{F}, z, \mathbf{Z}, \boldsymbol{\alpha}, \dot{z}, \dot{\mathbf{Z}}, \dot{\boldsymbol{\alpha}})\right] \cdot \mathbf{N} = \tau(\mathbf{X}, t), & (\mathbf{X}, t) \in \partial\Omega_0^{\mathbf{C}} \times [0, T] \\ z(\mathbf{X}, 0) = z_0(\mathbf{X}), & \mathbf{X} \in \Omega_0 \end{cases} \tag{10}$$

together with the evolution equation

$$\begin{cases} \mathcal{A}\{\dot{\boldsymbol{\alpha}}, \boldsymbol{\alpha}; \mathbf{F}, z, \mathbf{Z}\} = \mathbf{0}, & (\mathbf{X}, t) \in \Omega_0 \times [0, T] \\ \boldsymbol{\alpha}(\mathbf{X}, 0) = \boldsymbol{\alpha}_0(\mathbf{X}), & \mathbf{X} \in \Omega_0 \end{cases},$$

for the deformation field $\mathbf{y}(\mathbf{X}, t)$, the configurational field $z(\mathbf{X}, t)$, and the internal variables $\boldsymbol{\alpha}(\mathbf{X}, t)$, subject to the constraints $\det \mathbf{F}(\mathbf{X}, t) > 0$ and $0 \leq z(\mathbf{X}, t) \leq 1$. In (10), the possibly heterogeneous initial value of the configurational variable z throughout Ω_0 at $t = 0$ has been denoted by $z_0(\mathbf{X})$.

Remark 1 The Eqs. (9)–(10) are of Ginzburg-Landau type. In particular, $(9)_1$ stands for the balance of Newtonian forces driving the deformation, while $(10)_1$ stands for the balance of configurational forces driving the phase transitions. For a discussion of generalizations of the Ginzburg-Landau equations, also sometimes referred to as the Allen-Cahn equations, we refer the reader to Gurtin (1996).

3 Fracture and healing of elastomers as a solid-to-solid phase transition

In the sequel, we employ the preceding constitutive framework to directly re-derive the theory of fracture and healing of elastomers originally introduced in Kumar et al. (2018) as a generalization of the variational theory of brittle fracture of Francfort and Marigo (1998). We begin in Sect. 3.1 by spelling out the mechanisms by which elastomers can store and dissipate energy through deformation, fracture, and healing. These serve to dictate the specific functional forms of the two thermodynamic potentials (2). In Sects. 3.2 and 3.3, we further spell out the specific forms for the boundary conditions (7) on the configurational field and for the configurational external force $(8)_2$. Finally, we present the resulting complete theory in Sect. 3.4.

3.1 The mechanisms of energy storage and energy dissipation

The stored elastic energy of the original elastomer With the objective of being able to deal with compressible as well as with nearly incompressible elastomers, we take the elastic response of the elastomer of interest to be characterized, without loss of generality, by a free-energy density of the form

$$W(\mathbf{F}) + \kappa\, g(\mathbf{F}). \tag{11}$$

Here, κ is a non-negative material parameter (with unit *force/length*$^{N-1}$) that measures the compressibility of the elastomer: it is defined such that in the limit as $\kappa \to +\infty$, the elastomer is incompressible and its free-energy function (11) reduces to

$$\begin{cases} W(\mathbf{F}) & \text{if} \quad \det \mathbf{F} = 1 \\ +\infty & \text{otherwise} \end{cases}. \tag{12}$$

Basic physical considerations dictate that the functions W and g in (11) are objective, that is, $W(\mathbf{QF}) = W(\mathbf{F})$ and $g(\mathbf{QF}) = g(\mathbf{F})$ for all $\mathbf{Q} \in Orth^+$ and arbitrary $\mathbf{F}$, as well as satisfy the strong ellipticity condition $\partial^2 W(\mathbf{F})/\partial F_{ij} \partial F_{kl}\, A_j A_l b_i b_k + \kappa\, \partial^2 g(\mathbf{F})/\partial F_{ij} \partial F_{kl}\, A_j A_l b_i b_k > 0$ for all unit vectors $\mathbf{A}$ and $\mathbf{b}$ and arbitrary $\mathbf{F}$. For mathematical convenience and later use in the definition of a configurational external force c_{e}, we also assume that the function W satisfies the growth condition

$$W(\mathbf{F}) \to C|\mathbf{F}|^p \quad \text{as} \quad |\mathbf{F}| \to \infty \tag{13}$$

for some real exponent $p > 1$ and positive constant C (with unit *force/length*$^{N-1}$), where $|\mathbf{F}| = \sqrt{\mathbf{F}\cdot\mathbf{F}} = \sqrt{F_{ij}F_{ij}}$. As an example that we shall invoke in comparisons with experiments further below, we record the isotropic free-energy function (Lopez-Pamies 2010)

$$\sum_{r=1}^{2} \frac{N^{1-\beta_r}}{2\beta_r}\mu_r \left[(\mathbf{F}\cdot\mathbf{F})^{\beta_r} - N^{\beta_r} \right] - \sum_{r=1}^{2} \mu_r \ln(\det \mathbf{F}) + \frac{\kappa}{2}(\det \mathbf{F} - 1)^2 , \tag{14}$$

where we recall that N stands for the space dimension, and where β_r and μ_r ($r = 1, 2$) are real-valued material parameters (unitless and with unit *force/length*$^{N-1}$, respectively). Note that in the limit of incompressibility as $\kappa \to +\infty$, the free-energy function (14) reduces to

$$\begin{cases} \sum_{r=1}^{2} \dfrac{N^{1-\beta_r}}{2\beta_r}\mu_r \left[(\mathbf{F}\cdot\mathbf{F})^{\beta_r} - N^{\beta_r} \right] & \text{if} \quad \det \mathbf{F} = 1 \\ +\infty & \text{otherwise} \end{cases} ,$$

which is precisely of the advocated form (12).

The stored elastic energy of the fractured elastomer and the inter-phase regions We identify with the value of the configurational variable $z = 1$ the regions that are occupied by the original elastomer and with $z = 0$ the regions occupied by the fractured elastomer featuring vanishingly small stiffness. For definiteness, we take the elastic response of the latter and of the thin inter-phase regions wherein the configurational variable $0 < z < 1$ to be characterized by the free-energy density

$$W_{\mathcal{F}}(\mathbf{F}, z) = (z^2 + \eta_W)W(\mathbf{F}) + (z^2 + \eta_\kappa)\kappa\, g(\mathbf{F}) \tag{15}$$

with positive real numbers $\eta_\kappa \leq \eta_W \ll 1$.

Remark 2 The parameters η_W and η_κ introduced in (15) are small positive numbers that serve to quantify the vanishingly small stiffness of the regions of the elastomer that have undergone fracture; they are strictly positive so as to aid numerical tractability. When dealing with nearly incompressible elastomers, the compressibility parameter κ is typically 10^3 to 10^4 times larger than the smallest (principal) component of the initial modulus of elasticity $L_{ijkl} \doteq 1/2(\partial^2 W(\mathbf{I})/\partial F_{ij}\partial F_{kl} + \kappa\partial^2 g(\mathbf{I})/\partial F_{ij}\partial F_{kl})$ of the elastomer under consideration. Thus, to ensure that the fractured regions are indeed of vanishingly small stiffness, and, in particular, "empty" of an elastic fluid, the parameter η_κ should be chosen according to the rule $\eta_\kappa \leq \eta_W \min\{L_{ijkl}\}/\kappa$.

Remark 3 The choice of "degradation" functions $(z^2 + \eta_W)$ and $(z^2 + \eta_\kappa)$ used in (15) is one among a plethora of possible choices; see, e.g., Braides (1998), Bourdin et al. (2000), Pham et al. (2011), and Borden (2012). It is a choice that is standard in the literature and has the benefit of being mathematically simple.

The stored surface energy of the inter-phase regions In addition to storing energy through their elastic deformation, the thin inter-phase regions wherein $0 < z < 1$ may store "surface" energy. We associate to such an additional storage mechanism the free-energy density

$$W_{\mathcal{S}}(z, \mathbf{Z}, \boldsymbol{\alpha}) = k_{\mathcal{S}}(\boldsymbol{\alpha})\mathcal{S}_\varepsilon(z, \mathbf{Z})$$
$$\text{with} \quad \mathcal{S}_\varepsilon(z, \mathbf{Z}) = \frac{3}{8}\left(\frac{1-z}{\varepsilon} + \varepsilon\, \mathbf{Z}\cdot\mathbf{Z}\right), \tag{16}$$

where $k_{\mathcal{S}}(\boldsymbol{\alpha})$ is the material function taken to be

$$k_{\mathcal{S}}(\boldsymbol{\alpha}) = k^0_{\mathcal{S}} + H_{\mathcal{S}}\left(\alpha(\mathbf{X}, t^*(\mathbf{X}, t))\right) \tag{17}$$

in terms of the cumulative history of fracture and healing characterized by the pair $\boldsymbol{\alpha} = (\alpha, t^*)$ of memory variables

$$\alpha(\mathbf{X}, t) = \int_0^t |\dot{z}(\mathbf{X}, \tau)|\, \mathrm{d}\tau \qquad \text{and}$$
$$t^*(\mathbf{X}, t) = \sup\{\tau : \tau < t \text{ and } z(\mathbf{X}, \tau) = 1\}. \tag{18}$$

In expression (17), $k^0_{\mathcal{S}}$ is a non-negative material parameter (with unit *force/length*$^{N-2}$) and $H_{\mathcal{S}}(\cdot)$ is a bounded material function (obviously, also with unit *force/length*$^{N-2}$) satisfying the condition $H_{\mathcal{S}}(\alpha(\mathbf{X}, t^*(\mathbf{X}, 0))) = H_{\mathcal{S}}(0) = 0$ in the ground state at $t = 0$ and the lower bound $H_{\mathcal{S}}(\alpha(\mathbf{X}, t^*(\mathbf{X}, t))) \geq -k^0_{\mathcal{S}}$. Note that the memory variable $\alpha(\mathbf{X}, t)$ is nothing more than a counter that keeps track of the number of times that phase transitions (fracturing or healing) have occurred at a given material point $\mathbf{X}$ and time t. On the other hand, the memory variable t^* indicates the last time prior to the current time t that the elastomer was not fractured at a given material point $\mathbf{X}$.

Remark 4 The expression (16) is consistent with the pioneering approach to fracture of Griffith (1921), in that it states that the surface energy stored in the solid is proportional to the surface area that the thin inter-phase regions would occupy in the limit as $\varepsilon \to 0$. Indeed, the choice $(16)_2$ is one of a large class of possible N-dimensional volume density functions that can be utilized to approximate the area of $(N-1)$–dimensional surfaces contained in N-dimensional domains; see Chapter 4 in Braides (1998). The specific form $(16)_2$ has the merit that it is mathematically simple, it leads to sharp transitions of the configurational variable from $z = 1$ to $z = 0$, and possesses a number of other theoretical advantages over more conventional forms such as, for instance,

$$\mathcal{S}_\varepsilon(z, \mathbf{Z}) = \frac{1}{2}\left(\frac{(1-z)^2}{\varepsilon} + \varepsilon\, \mathbf{Z}\cdot\mathbf{Z}\right).$$

For a discussion of these, we refer the reader to Pham et al. (2011) and Sicsic and Marigo (2013).

The dissipated energy by the forward and the reverse phase transitions Finally, we take that both the forward and the reverse phase transitions—that is, again, the fracturing and the healing—may incur dissipation of energy. We associate to the forward (when $\dot{z} < 0$) and the reverse (when $\dot{z} > 0$) phase transitions the following dissipation potential

$$\phi_\varepsilon(\mathbf{Z}, \boldsymbol{\alpha}, \dot{z}, \dot{\mathbf{Z}}) = \begin{cases} \dfrac{3\,k_{\mathcal{F}}(\boldsymbol{\alpha})}{8}\left(-\dfrac{\dot{z}}{\varepsilon} + 2\varepsilon\, \mathbf{Z}\cdot\dot{\mathbf{Z}}\right) & \text{if} \quad \dot{z} \le 0 \\ -\dfrac{3\,k_{\mathcal{H}}(\boldsymbol{\alpha})}{8}\left(-\dfrac{\dot{z}}{\varepsilon} + 2\varepsilon\, \mathbf{Z}\cdot\dot{\mathbf{Z}}\right) & \text{if} \quad \dot{z} > 0 \end{cases} \tag{19}$$

with

$$\begin{aligned} k_{\mathcal{F}}(\boldsymbol{\alpha}) &= k^0_{\mathcal{F}} + H_{\mathcal{F}}\left(\alpha(\mathbf{X}, t^*(\mathbf{X}, t))\right), \\ k_{\mathcal{H}}(\boldsymbol{\alpha}) &= k^0_{\mathcal{H}} + H_{\mathcal{H}}\left(\alpha(\mathbf{X}, t^*(\mathbf{X}, t))\right). \end{aligned} \tag{20}$$

Analogous to the structure of the function $k_{\mathcal{S}}(\boldsymbol{\alpha})$ in expression (16), $k^0_{\mathcal{F}}$ and $k^0_{\mathcal{H}}$ in expressions (20) are non-negative material parameters (with unit *force/length*$^{N-2}$), while $H_{\mathcal{F}}(\cdot)$ and $H_{\mathcal{H}}(\cdot)$ are bounded material functions (with unit *force/length*$^{N-2}$) satisfying the conditions $H_{\mathcal{F}}\left(\alpha(\mathbf{X}, t^*(\mathbf{X}, 0))\right) = H_{\mathcal{F}}(0) = 0$ and $H_{\mathcal{H}}\left(\alpha(\mathbf{X}, t^*(\mathbf{X}, 0))\right) = H_{\mathcal{H}}(0) = 0$ in the ground state at $t = 0$, together with the lower bounds $H_{\mathcal{F}}\left(\alpha(\mathbf{X}, t^*(\mathbf{X}, t))\right) \ge -k^0_{\mathcal{F}}$ and $H_{\mathcal{H}}\left(\alpha(\mathbf{X}, t^*(\mathbf{X}, t))\right) \ge -k^0_{\mathcal{H}}$.

Remark 5 The choice of dissipation potential (19) is also consistent with Griffith's approach to fracture, as both branches in (19) state that the energy dissipated in fracturing or in healing is proportional to the created or healed surface area to which the thin inter-phase regions would reduce in the limit as $\varepsilon \to 0$. Note that the energy possibly dissipated during healing is, in general, different from that dissipated during fracture.

Remark 6 The constitutive choice that $k_{\mathcal{S}}(\boldsymbol{\alpha})$, $k_{\mathcal{F}}(\boldsymbol{\alpha})$, $k_{\mathcal{H}}(\boldsymbol{\alpha})$ are material functions of the cumulative history of fracture and healing and *not* merely material constants is motivated by recent experimental observations on a wide range of silicone elastomers discussed further below in Sect. 4. In particular, among a wealth of other possibilities[5], the specific prescriptions (17) and (20) with (18) are perhaps the simplest valid choices that are consistent with the experiments in describing that the ability of the elastomer to store and dissipate surface energy through fracturing and healing can evolve at a material point $\mathbf{X}$ after every *complete cycle* of fracturing and healing at that point. That is, after every cycle in which the configurational variable changes from $z(\mathbf{X}, t_1) = 1$ to $z(\mathbf{X}, t_2) = 0$ and back to $z(\mathbf{X}, t_3) = 1$ along a given loading path, the molecular structure of the elastomer at this point may adopt a different geometric arrangement and/or form different chemical bonds.

3.2 The boundary condition on the configurational field z

While the elastomer may be subjected to arbitrary mixed mechanical boundary conditions (6), we take the boundary conditions (7) on the configurational variable to be prescribed by zero Neumann boundary conditions over the entirety of the boundary, namely,

$$\mathbf{C}\cdot\mathbf{N} = 0, \quad (\mathbf{X}, t) \in \partial\Omega_0 \times [0, T]. \tag{21}$$

Physically, this implies that the fracturing and the healing of the elastomer is solely driven by the mechanical loads applied to it, and not by the direct imposition of a phase-transition stimulus on its boundary.

[5] For instance, it is possible that the elasticity—and not just the toughness—of the elastomer also evolves with the cumulative history of fracture and healing.

3.3 The configurational external force c_e

As is by now well established, when deformed, because of their typical near incompressibility, elastomers are prone to develop regions wherein the hydrostatic part of the stress is very large while, at the same time, the strain remains minute. More significantly, it is within such regions that fracture is likely to nucleate first; see, e.g., the analyses of Lefèvre et al. (2015) and Poulain et al. (2017). This is because the concentration of large hydrostatic stresses—in spite of the absence of strain and, hence, of strain energy—triggers the growth of the underlying internal microscopic defects, and thus, the nucleation of fracture at macroscopic length scales.

Now, while internal[6] defects inherent to elastomers can be of various natures, they are by and large randomly distributed and sub-micron in size (see, e.g., Gent 1990). These geometrical features effectively rule out the possibility of accounting for them explicitly in a macroscopic theory. Accordingly, the idea here is to account for their presence implicitly through the addition of a configurational external force c_e to the balance of configurational forces. In particular, we take

$$c_e(\mathbf{X}, t) = -\gamma\, z\, \frac{3^{\frac{p}{2}}}{|\mathbf{F}|^p} \left(\frac{\kappa}{3\, \det \mathbf{F}}\, \mathbf{F} \cdot \frac{\partial g}{\partial \mathbf{F}}(\mathbf{F}) \right). \tag{22}$$

The term inside the parenthesis in (22) corresponds to the hydrostatic part of the Cauchy stress $\mathbf{T} = (\det \mathbf{F})^{-1} \mathbf{S}\mathbf{F}^T$ associated with the compressibility parameter κ. The preceding quotient is a normalized measure of stretch, which takes the value of 1 in the absence of stretch when $\mathbf{F} \in Orth^+$. For large stretches, the quotient—and hence the force c_e—approaches zero with the inverse of the norm $|\mathbf{F}|^p$ that describes the growth (13) of the stored-energy function W. Notice as well that the force (22) vanishes within the fractured regions of the elastomer, where $z = 0$, consistent with physical expectations. Finally, the coefficient γ in (22) is a non-negative unitless parameter whose selection depends on the compressibility of the elastomer and on the geometry of the underlying microscopic defects. Specifically, as elaborated in the Appendix of Kumar et al. (2018), γ should be selected: (*i*) to be non-zero only for nearly incompressible elastomers and, more significantly, (*ii*) to take random values within a range, $[\gamma_{\min}, \gamma_{\max}]$ say, throughout the elastomer. The stochastic nature of the coefficient γ stems from the fact that its value depends on the size of the microscopic defects from which fracture initiates, and these are known to exhibit a range of random sizes in actual elastomers (Gent 1990).

Remark 7 The well-documented propensity of elastomers to first fracture in regions featuring a large hydrostatic stress but minute strain indicates that the *nucleation* of fracture in this class of solids cannot be captured through a balance *à la* Griffith between strain energy in the bulk and surface energy on the created new surfaces stemming from fracture. Indeed, such a balance would fail to pick out such regions because their contribution to the strain energy is negligible. The configurational external force (22) addresses this realization by adding part of the hydrostatic stress in the bulk to the competition between strain and surface energies. The particular form (22) does preserve, however, a balance *à la* Griffith for the *propagation* of fracture. This is so because $|\mathbf{F}|^p$ is large in and around a propagating crack front, and hence the force (22) effectively vanishes in those regions.

3.4 The proposed theory

Having identified the mechanisms of energy storage and dissipation, the boundary condition (21) on the configurational variable, and the configurational external force (22), we are now in a position to formulate the resulting theory of fracture and healing of elastomers within the general constitutive framework outlined in Sect. 2.

Indeed, for a given elastomer whose nonlinear elastic behavior is characterized by the stored-energy function (11), the two thermodynamic potentials (2) that dictate how it stores and dissipates energy through deformation, fracturing, and healing are given by

[6] In addition to internal microscopic defects throughout its *volume*, a given piece of elastomer will feature as well surface microscopic defects on its *boundary*. Depending on the geometry of the piece and the applied loading conditions, accounting for those may also be essential in order to describe correctly the nucleation of macroscopic fracture.

$$\psi(\mathbf{F}, z, \mathbf{Z}, \boldsymbol{\alpha}) = (z^2 + \eta_W)\, W(\mathbf{F}) + (z^2 + \eta_\kappa)\, \kappa\, g(\mathbf{F}) + \frac{3\, k_{\mathcal{S}}(\boldsymbol{\alpha})}{8} \left(\frac{1 - z}{\varepsilon} + \varepsilon\, \mathbf{Z} \cdot \mathbf{Z} \right) \tag{23}$$

and

tion field $\mathbf{y}(\mathbf{X}, t)$ and the configurational field $z(\mathbf{X}, t)$ describing the deformation and the nucleation and propagation of fracture and healing of the given elastomer of interest along any given loading path with prescribed deformation $\boldsymbol{\xi}(\mathbf{X}, t)$ on $\partial\Omega_0^{\mathbf{y}}$, prescribed nominal traction $\boldsymbol{\sigma}(\mathbf{X}, t)$ on $\partial\Omega_0^{\mathbf{S}}$, and prescribed body force $\mathbf{b}(\mathbf{X}, t)$ in Ω_0:

$$\begin{cases} \operatorname{Div}\left[(z^2 + \eta_W) \dfrac{\partial W}{\partial \mathbf{F}}(\mathbf{F}) + (z^2 + \eta_\kappa) \kappa \dfrac{\partial g}{\partial \mathbf{F}}(\mathbf{F}) \right] + \mathbf{b}(\mathbf{X}, t) = \mathbf{0},\ (\mathbf{X}, t) \in \Omega_0 \times [0, T] \\ \det \mathbf{F}(\mathbf{X}, t) > 0, \quad (\mathbf{X}, t) \in \Omega_0 \times [0, T] \\ \mathbf{y}(\mathbf{X}, t) = \boldsymbol{\xi}(\mathbf{X}, t), \quad (\mathbf{X}, t) \in \partial\Omega_0^{\mathbf{y}} \times [0, T] \\ \left[(z^2 + \eta_W) \dfrac{\partial W}{\partial \mathbf{F}}(\mathbf{F}) + (z^2 + \eta_\kappa) \kappa \dfrac{\partial g}{\partial \mathbf{F}}(\mathbf{F}) \right] \mathbf{N} = \boldsymbol{\sigma}(\mathbf{X}, t),\ (\mathbf{X}, t) \in \partial\Omega_0^{\mathbf{S}} \times [0, T] \end{cases} \tag{25}$$

and

$$\begin{cases} \operatorname{Div}\left[\varepsilon k(\dot{z}, \alpha, t^*) \mathbf{Z} \right] = \dfrac{8}{3} z\, (W(\mathbf{F}) + \kappa g(\mathbf{F})) + 4\gamma\, z\, \dfrac{3^{\frac{p-4}{2}}}{|\mathbf{F}|^p} \left(\dfrac{\kappa}{\det \mathbf{F}} \mathbf{F} \cdot \dfrac{\partial g}{\partial \mathbf{F}}(\mathbf{F}) \right) - \dfrac{k(\dot{z}, \alpha, t^*)}{2\varepsilon}, \\ \text{if } 0 < z(\mathbf{X}, t) < 1, \quad (\mathbf{X}, t) \in \Omega_0 \times [0, T] \\ \operatorname{Div}\left[\varepsilon k(\dot{z}, \alpha, t^*) \mathbf{Z} \right] \geq (\text{ resp. } \leq) \dfrac{8}{3} z\, (W(\mathbf{F}) + \kappa g(\mathbf{F})) + 4\gamma\, z\, \dfrac{3^{\frac{p-4}{2}}}{|\mathbf{F}|^p} \left(\dfrac{\kappa}{\det \mathbf{F}} \mathbf{F} \cdot \dfrac{\partial g}{\partial \mathbf{F}}(\mathbf{F}) \right) - \dfrac{k(\dot{z}, \alpha, t^*)}{2\varepsilon}, \\ \text{if } z(\mathbf{X}, t) = 1 (\text{ resp. } = 0), \quad (\mathbf{X}, t) \in \Omega_0 \times [0, T] \\ \mathbf{Z} \cdot \mathbf{N} = 0, \quad (\mathbf{X}, t) \in \partial\Omega_0 \times [0, T] \\ z(\mathbf{X}, 0) = z_0(\mathbf{X}), \quad \mathbf{X} \in \Omega_0 \end{cases} \tag{26}$$

with

$$k(\dot{z}, \alpha, t^*) = \begin{cases} k_{\mathcal{S}}(\boldsymbol{\alpha}) + k_{\mathcal{F}}(\boldsymbol{\alpha}) = k_{\mathcal{S}}^0 + k_{\mathcal{F}}^0 + H_{\mathcal{S}}\left(\alpha(\mathbf{X}, t^*(\mathbf{X}, t))\right) + H_{\mathcal{F}}\left(\alpha(\mathbf{X}, t^*(\mathbf{X}, t))\right) \text{ if } \dot{z} \leq 0 \\ k_{\mathcal{S}}(\boldsymbol{\alpha}) - k_{\mathcal{H}}(\boldsymbol{\alpha}) = k_{\mathcal{S}}^0 - k_{\mathcal{H}}^0 + H_{\mathcal{S}}\left(\alpha(\mathbf{X}, t^*(\mathbf{X}, t))\right) - H_{\mathcal{H}}\left(\alpha(\mathbf{X}, t^*(\mathbf{X}, t))\right) \text{ if } \dot{z} > 0 \end{cases},$$

$$\phi(\mathbf{Z}, \boldsymbol{\alpha}, \dot{z}, \dot{\mathbf{Z}}) = \begin{cases} \dfrac{3\, k_{\mathcal{F}}(\boldsymbol{\alpha})}{8} \left(-\dfrac{\dot{z}}{\varepsilon} + 2\varepsilon\, \mathbf{Z} \cdot \dot{\mathbf{Z}} \right) & \text{if } \dot{z} \leq 0 \\ -\dfrac{3\, k_{\mathcal{H}}(\boldsymbol{\alpha})}{8} \left(-\dfrac{\dot{z}}{\varepsilon} + 2\varepsilon\, \mathbf{Z} \cdot \dot{\mathbf{Z}} \right) & \text{if } \dot{z} > 0 \end{cases}. \tag{24}$$

Recall that $\boldsymbol{\alpha}$ stands for the pair of scalar internal variables (18). Note also that the dissipation potential (24) is independent of $\mathbf{F}$, z, and $\dot{\boldsymbol{\alpha}}$, hence the exclusion of these variables in the arguments of ϕ.

Making use of the above two thermodynamic potentials and indicated boundary conditions and configurational external force in the general governing Eqs. (9)–(10), with a suitable interpretation of the partial derivative of (24) with respect to the argument $\dot{z}$, the following governing equations are generated for the deforma-

where, again, we recall that $\alpha(\mathbf{X}, t)$ and $t^*(\mathbf{X}, t)$ stand for the memory variables (18).

The governing Eqs. (25)–(26) are precisely those introduced in Kumar et al. (2018). For a thorough discussion of their key theoretical and practical aspects, as well as of their numerical implementation in the physically relevant contexts of $N = 2$ and 3 space dimensions, we refer the interested reader to Subsection 3.3 and Section 4 in Kumar et al. (2018). Here, we find it convenient to record a few practical remarks concerning their physical significance and use.

Remark 8 When constructing numerical solutions for (25)–(26), it is difficult to enforce *a priori* the satisfaction of the inequalities $\det \mathbf{F}(\mathbf{X}, t) > 0$ and $0 \leq z(\mathbf{X}, t) \leq 1$. An expedient approach to address this

difficulty is to employ a procedure routinely followed in finite elasticity, namely, to restrict attention to stored-energy functions $W(\mathbf{F})$ with the property that

$$W(\mathbf{F}) \to \infty \quad \text{as} \quad \det \mathbf{F} \to 0+, \tag{27}$$

and, analogously, to add to the free-energy density ψ the penalty function

$$W_\nu(z) = \frac{\nu}{2}\left[(|z| - z)^2 + (|1 - z| - (1 - z))^2\right], \tag{28}$$

where ν is a real-valued parameter (with unit *force/length*$^{N-1}$) to be selected so that $\nu \gg \max\{k(\dot{z}, \alpha, t^*)\}/\varepsilon$. While the property (27) penalizes the violation of the inequality $\det \mathbf{F}(\mathbf{X}, t) > 0$, the addition of the function (28) to the free-energy density (23) penalizes the violation of the inequalities $0 \leq z(\mathbf{X}, t) \leq 1$; see, e.g., Parikh and Boyd (2013) for a detailed discussion of this type of approach, referred to as the Moreau-Yosida regularization in the optimization literature. With the above modifications, the governing equations can be rewritten free of the inequality constraints $\det \mathbf{F}(\mathbf{X}, t) > 0$ and $0 \leq z(\mathbf{X}, t) \leq 1$ as

$$\begin{cases} \operatorname{Div}\left[(z^2 + \eta_W)\dfrac{\partial W}{\partial \mathbf{F}}(\mathbf{F}) + (z^2 + \eta_\kappa)\kappa\dfrac{\partial g}{\partial \mathbf{F}}(\mathbf{F})\right] \\ +\mathbf{b}(\mathbf{X}, t) = \mathbf{0}, \quad (\mathbf{X}, t) \in \Omega_0 \times [0, T] \\ \mathbf{y}(\mathbf{X}, t) = \boldsymbol{\xi}(\mathbf{X}, t), \quad (\mathbf{X}, t) \in \partial\Omega_0^{\mathbf{y}} \times [0, T] \\ \left[(z^2 + \eta_W)\dfrac{\partial W}{\partial \mathbf{F}}(\mathbf{F}) + (z^2 + \eta_\kappa)\kappa\dfrac{\partial g}{\partial \mathbf{F}}(\mathbf{F})\right]\mathbf{N} \\ = \boldsymbol{\sigma}(\mathbf{X}, t), \quad (\mathbf{X}, t) \in \partial\Omega_0^{\mathbf{S}} \times [0, T] \end{cases}$$

and

$$\begin{cases} \operatorname{Div}\left[\varepsilon k(\dot{z}, \alpha, t^*)\mathbf{Z}\right] = \dfrac{8}{3} z\,(W(\mathbf{F}) + \kappa g(\mathbf{F})) \\ +4\gamma\, z\,\dfrac{3^{\frac{p-4}{2}}}{|\mathbf{F}|^p}\left(\dfrac{\kappa}{\det \mathbf{F}}\,\mathbf{F} \cdot \dfrac{\partial g}{\partial \mathbf{F}}(\mathbf{F})\right) - \dfrac{k(\dot{z}, \alpha, t^*)}{2\varepsilon} \\ +\dfrac{8}{3}\nu\,(2z - 1 + |1 - z| - |z|), \quad (\mathbf{X}, t) \in \Omega_0 \times [0, T] \\ \mathbf{Z} \cdot \mathbf{N} = 0, \quad (\mathbf{X}, t) \in \partial\Omega_0 \times [0, T] \\ z(\mathbf{X}, 0) = z_0(\mathbf{X}), \quad \mathbf{X} \in \Omega_0 \end{cases}.$$

Remark 9 For a given problem of interest, the regularization parameter ε in the governing Eq. $(26)_{1-2}$ should be selected to be much smaller than the smallest characteristic length scale of the domain Ω_0 occupied by the elastomer in its initial configuration at time $t = 0$; for example, in the Gent-Park-type problem schematically depicted in Fig. 2, ε should be selected to be much smaller than the initial gap H_0 between the beads. Provided that ε is selected to be sufficiently small as described above, its actual value has no significant effect on the solution of the governing Eqs. (25)–(26) for the deformation field $\mathbf{y}(\mathbf{X}, t)$ and the configurational field $z(\mathbf{X}, t)$, so long as the force parameter γ be calibrated consistently for the chosen value of ε. This dependence of γ on ε is elaborated further in Remark 11 below.

Remark 10 The right-hand side of the governing Eq. $(26)_{1-2}$ makes apparent the precise competition between bulk and surface quantities that drive the nucleation and propagation of fracture and healing in the elastomer. Indeed, we remark that nucleation and propagation of fracture will occur at a material point $\mathbf{X}$ whenever the strain energy, as characterized by $W(\mathbf{F}) + \kappa g(\mathbf{F})$, together with the hydrostatic stress relative to the amount of stretch, as characterized by $\gamma\, 3^{\frac{p-4}{2}}/|\mathbf{F}|^p$ $((\kappa/\det \mathbf{F})\,\mathbf{F} \cdot \partial g(\mathbf{F})/\partial \mathbf{F})$, is sufficiently large relative to the fracture toughness $k_{\mathcal{S}}(\boldsymbol{\alpha}) + k_{\mathcal{F}}(\boldsymbol{\alpha})$ of the elastomer at that material point. By the same token, healing will occur at a material point $\mathbf{X}$ if the same combination of strain energy and stress is sufficiently small relative to the healing toughness $k_{\mathcal{S}}(\boldsymbol{\alpha}) - k_{\mathcal{H}}(\boldsymbol{\alpha})$ at that material point.

It is insightful to further recognize more explicitly from the governing Eq. $(26)_{1-2}$ that nucleation of fracture may first initiate—that is, the configurational variable may first evolve from 1 to strictly less than 1—at a material point $\mathbf{X}$ whenever the following simple *algebraic* condition is satisfied:

$$\frac{8}{3}\,(W(\mathbf{F}) + \kappa g(\mathbf{F})) + 4\gamma\,\frac{3^{\frac{p-4}{2}}}{|\mathbf{F}|^p}\left(\frac{\kappa}{\det \mathbf{F}}\,\mathbf{F} \cdot \frac{\partial g}{\partial \mathbf{F}}(\mathbf{F})\right) - \frac{k_{\mathcal{S}}(\boldsymbol{\alpha}) + k_{\mathcal{F}}(\boldsymbol{\alpha})}{2\varepsilon} = 0. \tag{29}$$

Consistent with the analyses of Lefèvre et al. (2015) and Poulain et al. (2017, 2018) of the classical experiments of Gent and collaborators as well as of analogous new experiments at higher spatio-temporal resolution, the "onset of cavitation" criterion (29) depends fundamentally on the non-Gaussian stiffening of the elastomer (through $W(\mathbf{F})$ and $|\mathbf{F}|^p$ in the first and second terms), on its fracture properties (through $k_{\mathcal{S}}(\boldsymbol{\alpha}) + k_{\mathcal{F}}(\boldsymbol{\alpha})$ in the third term), and on the nature of its inherent microscopic defects (through the force parameter γ in the second term).

Remark 11 The governing Eqs. (25)–(26) comprise three constitutive inputs: (i) the material function $W(\mathbf{F})+\kappa g(\mathbf{F})$, which characterizes the nonlinear elastic response of the elastomer, including its compressibility, (ii) the toughness function $k(\dot{z},\alpha,t^*)$, which characterizes the initial as well as the evolving resistance of the elastomer to fracture and to heal, and (iii) the force parameter γ, which characterizes the presence of defects in the elastomer from which macroscopic fracture nucleates.

For a given elastomer of interest, the "top-down" calibration of these three constitutive inputs requires four different sets of macroscopic experimental data. *Grosso modo*, first, the material function $W(\mathbf{F})+\kappa g(\mathbf{F})$ can be calibrated from standard quasistatic uniaxial, biaxial, and/or shear mechanical tests; these tests must be carried out up to sufficiently large deformations in order to determine the non-Gaussian stiffening of the elastomer (*i.e.*, the exponent p).

Second, the initial values $k_{\mathcal{S}}^0+k_{\mathcal{F}}^0$ and $k_{\mathcal{S}}^0-k_{\mathcal{H}}^0$ of the two branches of the toughness function $k(\dot{z},\alpha,t^*)$ can be calibrated from a loading/unloading test on a pre-cracked specimen of the elastomer. We recall that the initial value of fracture toughness $k_{\mathcal{S}}^0+k_{\mathcal{F}}^0$ is nothing more than the conventional critical energy release rate G_c of the elastomer. We also recall that if healing does *not* occur, then it suffices to set $k_{\mathcal{S}}^0-k_{\mathcal{H}}^0\leq 0$; see Remark 4 in Kumar et al. (2018).

Third, the material functions $H_{\mathcal{S}}\left(\alpha(\mathbf{X},t^*(\mathbf{X},t))\right)+H_{\mathcal{F}}\left(\alpha(\mathbf{X},t^*(\mathbf{X},t))\right)$ and $H_{\mathcal{S}}\left(\alpha(\mathbf{X},t^*(\mathbf{X},t))\right)-H_{\mathcal{H}}\left(\alpha(\mathbf{X},t^*(\mathbf{X},t))\right)$ that describe the evolution of $k(\dot{z},\alpha,t^*)$ in fracture and in healing must be calibrated from multiple cycles of loading/unloading tests on pre-cracked specimens. An alternative procedure is to use the experiments of the type presented below in Sect. 4 in order to infer these material functions.

Fourth and finally, the force parameter γ can be calibrated from mechanical tests, such as the so-called poker-chip and the Gent-Park tests, that allow for a direct observation of the nucleation of fracture at a spatial resolution of a few microns. Here, it is important to emphasize that the calibration of the force parameter γ—as opposed to the material parameters and material functions discussed above—is dependent on the value used for the regularization parameter ε. Specifically, as can be inferred from the nucleation criterion (29), smaller values of ε typically lead to larger values of γ.

Section 7 in Kumar et al. (2018) provides a first example of the calibration of the material function $W(\mathbf{F})+\kappa g(\mathbf{F})$, the initial value of the fracture toughness $k_{\mathcal{S}}^0+k_{\mathcal{F}}^0$, and the force parameter γ for two of the silicone elastomers investigated in Poulain et al. (2017). In the following section, we present a more complete example also involving the calibration of the initial healing toughness $k_{\mathcal{S}}^0-k_{\mathcal{H}}^0$ and the material functions $H_{\mathcal{S}}\left(\alpha(\mathbf{X},t^*(\mathbf{X},t))\right)+H_{\mathcal{F}}\left(\alpha(\mathbf{X},t^*(\mathbf{X},t))\right)$ and $H_{\mathcal{S}}\left(\alpha(\mathbf{X},t^*(\mathbf{X},t))\right)-H_{\mathcal{H}}\left(\alpha(\mathbf{X},t^*(\mathbf{X},t))\right)$.

We close this remark by pointing out that the "bottom-up" calibration of the material function $W(\mathbf{F})+\kappa g(\mathbf{F})$ is certainly possible; see, e.g., Treloar (2005), Alicandro et al. (2011), Gloria et al. (2014) and references therein. On the other hand, it is not clear whether this is also true about the toughness function $k(\dot{z},\alpha,t^*)$ and the force parameter γ. The Appendix in Kumar et al. (2018) suggests that there might be indeed a direct and mathematically rigorous connection between these macroscopic constitutive inputs and the molecular make up of the elastomer, but this is yet to be proved or disproved.

4 Comparisons with the experiments of Poulain et al. (2018)

In this final section, we make use of the above-rederived theory to examine experimental results recently reported in Poulain et al. (2018). As schematically depicted in Fig. 2, the experiments in that work consist in cyclically stretching/unstretching a block of transparent PDMS elastomer embedding two spherical glass beads that are firmly bonded to the elastomer and aligned in the direction of the applied load. For an improved control of the applied loads, following one of the experimental setups introduced in Poulain et al. (2017), the specimens feature two metallic strips that are bonded to the beads and extend all the way to the grips where the loads are applied. The diameter D_0 of the beads is in the order of millimeters, the initial gap H_0 between them is sub-millimetric, and, more significantly, an optical microscope is used to monitor the various processes of nucleation and propagation of fracture and healing at a spatial resolution of about 1 μm and a temporal resolution of 15 frames per second.

For definiteness, we focus on the experiment presented in Section 3 of Poulain et al. (2018). The specimen there is made of a PDMS elastomer with a 30:1 ratio of base to curing agent, the glass beads have a diameter of $D_0=3.170$ mm and are set apart by an

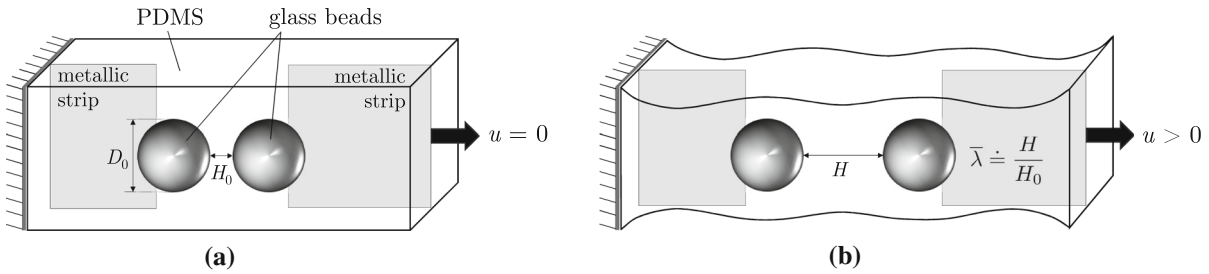

Fig. 2 Schematics of the specimen geometry, in **a** its initial configuration and in **b** a deformed configuration, and the applied boundary conditions used in the experiments of Poulain et al. (2018). The experiments are parameterized in terms of the average stretch across the gap between the beads identified in part (**b**): $\overline{\lambda} \doteq H/H_0$

initial gap of $H_0 = 0.162$ mm. Accordingly, in our theoretical description of this experiment, we make use of a free-energy function $W(\mathbf{F}) + \kappa g(\mathbf{F})$ of the form (14) with material parameters

$$\beta_1 = -1.02103, \quad \beta_2 = 1.39107, \quad \mu_1 = 0.01857\,\text{MPa},$$
$$\mu_2 = 0.03192\,\text{MPa}, \quad \kappa = 10^3(\mu_1 + \mu_2) = 56\,\text{MPa} \tag{30}$$

to characterize the nonlinear elastic[7] response of the underlying PDMS. Furthermore, we make use of the toughness function

$$k(\dot{z}, \alpha, t^*) = \begin{cases} \left[20 + \alpha(\mathbf{X}, t^*(\mathbf{X}, t))\right] \text{ J/m}^2 & \text{if } \dot{z} \le 0 \\ \left[5 - 0.1875\,\alpha(\mathbf{X}, t^*(\mathbf{X}, t))\right] \text{ J/m}^2 & \text{if } \dot{z} > 0 \end{cases} \tag{31}$$

and a stochastic force parameter γ that takes values in the range

$$\gamma \in [1.6, 1.8] \tag{32}$$

randomly throughout the region occupied by the PDMS. We remark that the material parameters (30) were obtained from independent quasistatic uniaxial stress-stretch data for PDMS 30:1. On the other hand, since no independent experiments on pre-cracked specimens on this type of PDMS are available, the form and material parameters of the toughness function (31), much like the range of values of the force parameter (32), were selected so as to lead to results that match with the experimental observations, while, at the same time, be plausible. Finally, we note that all the theoretical results that follow were computed with no body forces, $\mathbf{b}(\mathbf{X}, t) = \mathbf{0}$, and parameters $\varepsilon = 5\ \mu$m, $\eta_W = 10^{-3}$, $\eta_\kappa = 10^{-6}$, in an uniform axisymmetric finite-element discretization of size $h = \varepsilon/3 = 1.67\ \mu$m in the PDMS region between the beads. The interested reader is referred to Section 4 of Kumar et al. (2018) for further details regarding the numerical method of solution.

The first cycle of stretching/unstretching We begin by examining the experimental results obtained during the stretching of the specimen in the first cycle of the loading. To that effect, Fig. 3 shows snapshots of the PDMS region between the beads at three increasing values of the average stretch $\overline{\lambda}$, alongside corresponding contour plots of the configurational variable, in the undeformed and the deformed configurations, computed from the theory.

The central observation from Fig. 3 is that the theory describes fairly accurately all the experimental observations, from the nucleation of a crack near the pole of the right bead, to its growth and sustained deformed conical shape, to its subsequent growth and deformation into a cylindrical shape upon further loading. We emphasize that the theory is able to describe the nucleation of fracture near the pole of one of the beads, as opposed to near the pole of the opposite bead, because the force parameter γ takes on random values in the range (32) throughout the PDMS elastomer and, in particular, happens to be slightly larger near the pole of the right bead for the specific realization shown in Fig. 3. As discussed in the Appendix of Kumar et al. (2018), this would imply that the underlying microscopic defect from which fracture initiates in the actual

[7] Here, it is important to emphasize that the PDMS elastomer used in the experiment, featuring a 30:1 ratio of base to curing agent, is a solid capable of some viscous dissipation. Consequently, its idealization as a nonlinear elastic solid in the theory may cause some disagreement between the predictions from the theory and the experimental observations.

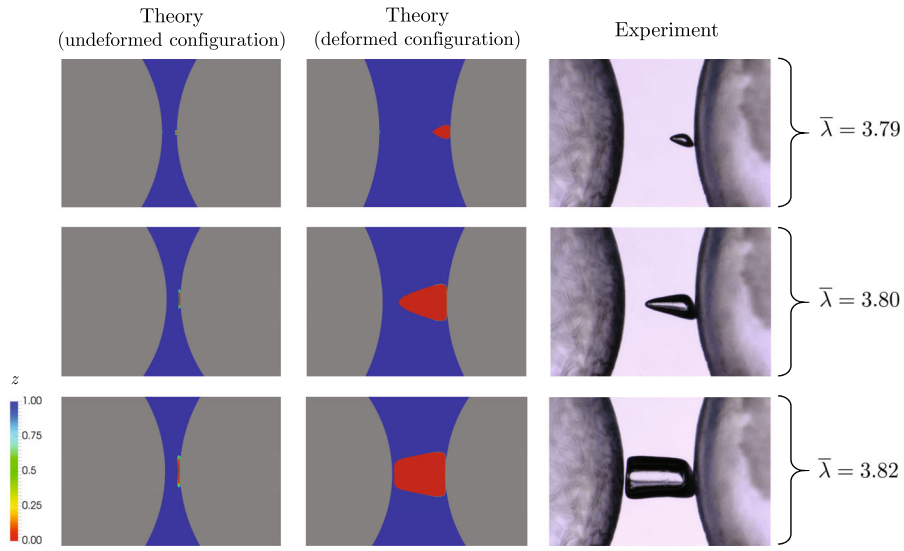

Fig. 3 Comparison of the theory with the experiment in Section 3 of Poulain et al. (2018) for a specimen, with bead diameter $D_0 = 3.170$ mm and gap between the beads $H_0 = 0.162$ mm, made of a PDMS elastomer with a 30:1 ratio of base to curing agent. The experimental results show snapshots of the PDMS region between the beads at three increasing values of the average stretch $\overline{\lambda}$ during the *stretching* in the *first loading cycle*. The contour plots show the corresponding theoretical results for the configurational variable in the undeformed and the deformed configurations

Fig. 4 Comparison of the theory with the experiment at three decreasing values of the average stretch $\overline{\lambda}$ during the *unstretching* in the *first loading cycle*

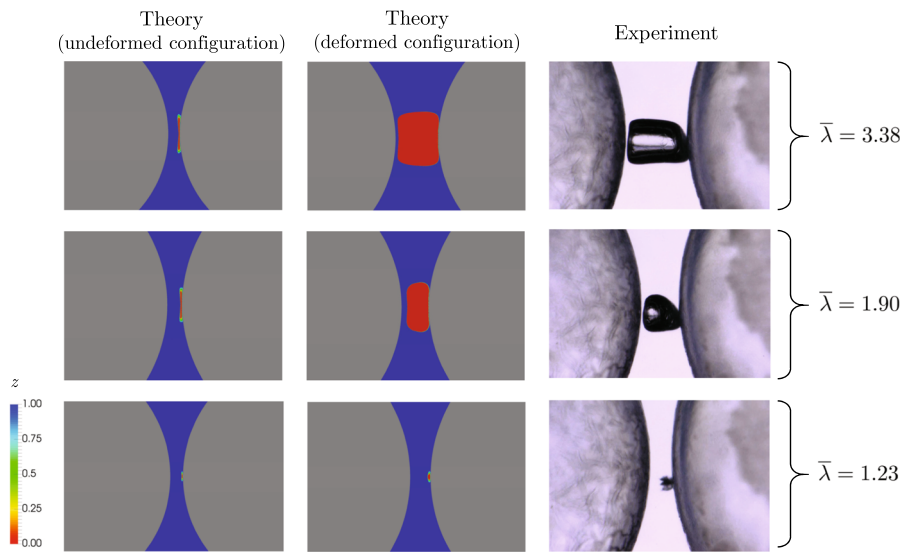

elastomer is slightly larger than its counterpart near the opposite bead.

In a similar fashion to Fig. 3, Fig. 4 shows comparisons between the theory and the experiment at three decreasing values of the average stretch $\overline{\lambda}$ between the beads during the unstretching of the specimen in the first cycle of the loading. In this set of comparisons too, the theory is seen to describe correctly the main experimental observations, namely, that the crack completely heals upon unstretching, but that it does so following a different path than the one followed during the stretching. However, there are some differences between the deformed shapes of the cracks predicted by the theory and those observed in the experiment. These are likely due to the facts that the simulations are axisymmetric (and *not* fully 3D) and that the theory

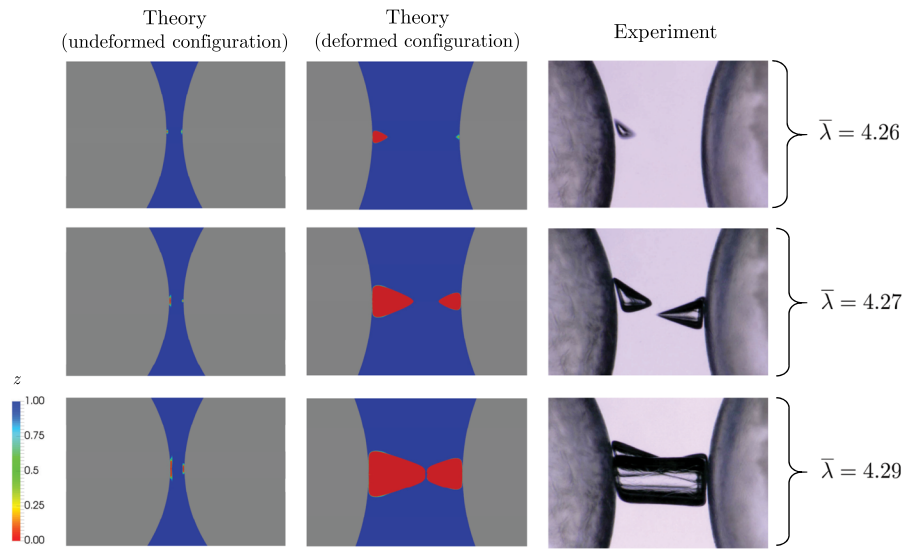

Fig. 5 Comparison of the theory with the experiment at three increasing values of the average stretch $\overline{\lambda}$ during the *stretching* in the *second loading cycle*

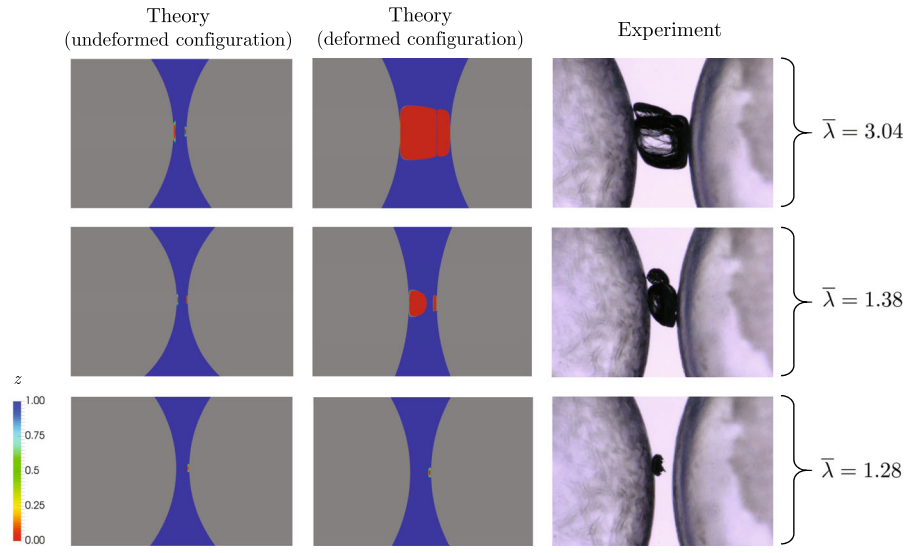

Fig. 6 Comparison of the theory with the experiment at three decreasing values of the average stretch $\overline{\lambda}$ during the *unstretching* in the *second loading cycle*

does not account for viscous effects, which may play a role during the healing process in the experiment. Non-axisymmetric and viscous effects notwithstanding, in view of the significantly smaller initial value of the toughness for healing ($k_{\mathcal{S}}^0 - k_{\mathcal{H}}^0 = 5$ J/m^2) than that for fracture ($k_{\mathcal{S}}^0 + k_{\mathcal{F}}^0 = 20$ J/m^2) assumed in the theoretical results[8], the comparisons in Fig. 4 suggest that the crack in the actual experiment simply deforms during most of the unstretching, and it only starts to heal once the specimen is almost completely unstretched.

The second cycle of stretching/unstretching We now turn the focus to the experimental results obtained during the second cycle of the stretching/unstretching of the specimen. Accordingly, Figs. 5 and 6 present analogous results to those displayed in Figs. 3 and 4 for this second cycle.

[8] We recall that smaller positive values in the healing branch of the toughness function $k(\dot{z}, \alpha, t^*)$ imply that the material exhibits a higher resistance to heal. Again, non-positive values imply that healing is prohibited altogether; see Remark 4 in Kumar et al. (2018).

Starting with Fig. 5, we remark that the first nucleation of a crack in the experiment occurs near the pole of the left bead at the stretch $\overline{\lambda} = 4.26$, as opposed to near the pole of the right bead at the significantly smaller stretch $\overline{\lambda} = 3.79$, about where and when fracture first nucleated during the first cycle of the loading. Upon further loading, a second crack is nucleated near the pole of the right bead at about the same location where a crack first appeared during the first cycle of the loading. The theory is able to describe this intricate behavior thanks to the choice of evolving toughness function (31). Indeed, according to (31), the fracture toughness in the regions of the PDMS that experience a complete cycle of fracture and healing *increases* by 10% of its initial value of 20 J/m^2. This modest increase is enough to delay the nucleation of fracture near the pole of the right bead from $\overline{\lambda} = 3.79$ to $\overline{\lambda} = 4.27$, as observed in the experiment. We also notice that the location and propagation of the nucleated cracks predicted by the theory are somewhat different from those observed in the experiment. This discrepancy is, again, presumably due to the fact that the simulations were performed on an axisymmetric discretization, and not on a full 3D one.

Similar to the results shown in Fig. 4 for the first cycle of the loading, Fig. 6 shows that the cracks completely heal upon unstretching the specimen and that they do so by following a different path than the one followed during the stretching. We remark that the theory is able to describe not only this behavior but also the fine experimental observation that the second nucleated crack heals after the first one because of the choice of toughness function (31). This choice entails that the healing toughness in the regions of the PDMS that experience a complete cycle of fracture and healing *decreases* by 7.5% of its initial value of 5 J/m^2. This modest decrease is enough to delay the healing of the second nucleated crack until after the first one has completely healed. Finally we note that, much like in the first unstretching, viscous effects may play a role in the second unstretching of the specimen. This, together with the axisymmetric nature of the simulation, might explain the differences between the deformed shapes of the cracks predicted by the theory and those observed in the experiment.

We close by noting that the files M_1 and M_2 in the supplementary material provide videos of the simulations shown in Figs. 3 through 6 of the first and second loading cycles.

Acknowledgements Support for this work by the National Science Foundation through the Grant DMS–1615661 is gratefully acknowledged.

References

Alicandro R, Cicalese M, Gloria A (2011) Integral representation results for energies defined on stochastic lattices and application to nonlinear elasticity. Arch Ration Mech Anal 200:881–943

Borden MJ (2012) Isogeometric analysis of phase-field models for dynamic brittle and ductile fracture. University of Texas at Austin Ph.D. Thesis

Bourdin B, Francfort GA, Marigo JJ (2000) Numerical experiments in revisited brittle fracture. J Mech Phys Solids 48:797–826

Bourdin B, Francfort GA, Marigo JJ (2008) The variational approach to fracture. J Elast 91:5–148

Braides A (1998) Approximation of free-discontinuity problems. Springer, Berlin

Francfort GA, Marigo JJ (1998) Revisiting brittle fracture as an energy minimization problem. J Mech Phys Solids 46:1319–1342

Fried E, Gurtin ME (1994) Dynamic solid-solid transitions with phase characterized by an order parameter. Physica D 72:287–308

Gent AN (1990) Cavitation in rubber: a cautionary tale. Rubber Chem Technol 63:49–53

Gent AN, Lindley PB (1959) Internal rupture of bonded rubber cylinders in tension. Proc R Soc A 249:195–205

Gent AN, Park B (1984) Failure processes in elastomers at or near a rigid inclusion. J Mater Sci 19:1947–1956

Gloria A, Le Tallec P, Vidrascu M (2014) Foundation, analysis, and numerical investigation of a variational network-based model for rubber. Continuum Mech Thermodyn 26:1–31

Griffith AA (1921) The phenomena of rupture and flow in solids. Philos Trans R Soc Lond A 221:163–198

Gurtin ME (1996) Generalized Ginzburg–Landau and Cahn–Hilliard equations based on a microforce balance. Physica D 92:178–192

Kumar A, Lopez-Pamies O (2016) On the two-potential constitutive modelling of rubber viscoelastic materials. Comptes Rendus Mecanique 344:102–112

Kumar A, Aranda-Iglesias D, Lopez-Pamies O (2017) Some remarks on the effects of inertia and viscous dissipation in the onset of cavitation in rubber. J Elast 126:201–213

Kumar A, Francfort GA, Lopez-Pamies O (2018) Fracture and healing of elastomers: a phase-transition theory and numerical implementation. J Mech Phys Solids 112:523–551

Lefèvre V, Ravi-Chandar K, Lopez-Pamies O (2015) Cavitation in rubber: an elastic instability or a fracture phenomenon? Int J Fracture 192:1–23

Lopez-Pamies O (2010) A new I_1-based hyperelastic model for rubber elastic materials. Comptes Rendus Mecanique 338:3–11

Mullins L (1959) Rupture of rubber. IX. Role of hysteresis in the tearing of rubber. Trans Inst Rubber Ind 35:213–222

Nguyen QS, Andrieux S (2005) The non-local generalized standard approach: a consistent gradient theory. Comptes Rendus Mecanique 333:139–145

Parikh N, Boyd S (2013) Proximal algorithms. Found Trends Optim 1:123–231

Pham K, Amor H, Marigo JJ, Maurini C (2011) Gradient damage models and their use to approximate brittle fracture. Int J Damage Mech 20:618–652

Poulain X, Lefèvre V, Lopez-Pamies O, Ravi-Chandar K (2017) Damage in elastomers: nucleation and growth of cavities, micro-cracks, and macro-cracks. Int J Fracture 205:1–21

Poulain X, Lopez-Pamies O, Ravi-Chandar K (2018) Damage in elastomers: healing of internally nucleated cavities and micro-cracks. Soft Matter 14:4633–4640

Sicsic P, Marigo JJ (2013) From gradient damage laws to Griffith's theory of crack propagation. J Elast 113:55–74

Treloar LRG (2005) The physics of rubber elasticity. Clarendon Press, Oxford

Ziegler H, Wehrli C (1987) The derivation of constitutive relations from the free energy and the dissipation function. Adv Appl Mech 25:183–238